

# Fast Directional Spatially Localized Spherical Harmonic Transform

Zubair Khalid, *Student Member, IEEE*, Rodney A. Kennedy, *Fellow, IEEE*, Salman Durrani, *Senior Member, IEEE*, Parastoo Sadeghi, *Senior Member, IEEE* and Jason D. McEwen, *Member, IEEE*

**Abstract**—For signals defined on the sphere, we develop a tool to project the signal onto the joint spatio-spectral domain. We revisit the definition of the spatially localized spherical harmonic transform (SLSHT) from the literature, where azimuthally symmetric window functions were used for spatial localization. We propose a directional (i.e., azimuthally asymmetric) window function for spatial localization, which enables the transform to reveal localized directional content in the spatio-spectral domain; hence, we call the proposed transform the directional SLSHT and the spatio-spectral representation as the directional SLSHT distribution. We present a fast algorithm for the efficient computation of the transform, which is required for practical applications. We study the accuracy and speed of our fast algorithm and show that it achieves very good numerical accuracy, with numerical errors at the level of floating point precision. Finally, an example is presented to illustrate the capability of the directional SLSHT to resolve localized directional features in the spatio-spectral domain.

**Index Terms**—Signal analysis, spherical harmonics, 2-sphere.

## I. INTRODUCTION

Signals that are inherently defined on the sphere appear in various fields of science and engineering, such as medical image analysis [1], geodesy [2], computer graphics [3], planetary science [4], electromagnetic inverse problems [5], cosmology [6], 3D beamforming [7] and wireless channel modeling [8]. In order to analyze

and process signals on the sphere, many signal processing techniques have been extended from the Euclidean domain to the spherical domain [2], [9]–[23].

Due to the ability of wavelets to resolve localized signal content in both space and scale, wavelets have been extensively investigated for analyzing signals on the sphere [9], [13]–[15], [19]–[23] and have been utilized in various applications (e.g., in astrophysics [24]–[29] and geophysics [4], [30], [31]). Some of the wavelet techniques on the sphere also incorporate directional phenomena in the spatial-scale decomposition of a signal (e.g., [21]–[23]). As an alternative to spatial-scale decomposition, spatio-spectral (spatial-spectral) techniques have also been developed and applied for localized spectral analysis, spectral estimation and spatially varying spectral filtering of signals [10], [12], [18], [32], [33]. The spectral domain is formed through the spherical harmonic transform which serves as a counterpart of the Fourier transform for signals on the sphere [5], [34]–[36].

The localized spherical harmonic transform, composed of spatial windowing followed by spherical harmonic transform, was first devised in [18] for localized spectral analysis. We note that the localized spherical harmonic transform was defined in [18] for azimuthally asymmetric (i.e., directional) window functions, however, it was applied and investigated for azimuthally symmetric functions only. Furthermore, a spectrally truncated azimuthally symmetric window function was used for spatial localization [18]. Due to spectral truncation, the window used for spatial localization may not be concentrated in the region of interest. This issue was resolved in [32], where azimuthally symmetric eigenfunctions obtained from the Slepian concentration problem on the sphere were used as window functions (the Slepian concentration problem is studied for arbitrary regions on the sphere in [2]). Following [18], the spatially localized spherical harmonic transform (SLSHT) for signals on the sphere has been devised in [10] to obtain the spatio-spectral representation of signals for azimuthally symmetric window functions, where the effect of different window functions on the SLSHT distribution is studied.

Z. Khalid, R. A. Kennedy, S. Durrani and P. Sadeghi are with the Research School of Engineering, College of Engineering and Computer Science, The Australian National University, Canberra, Australia. J. D. McEwen is with the Department of Physics and Astronomy, University College London, London WC1E 6BT, UK.

Z. Khalid, R. A. Kennedy and P. Sadeghi are supported by the Australian Research Council's Discovery Projects funding scheme (Project No. DP1094350). J. D. McEwen is supported by a Newton International Fellowship from the Royal Society and the British Academy.

E-mail: zubair.khalid@anu.edu.au (Z. Khalid)

E-mail: rodney.kennedy@anu.edu.au (R. A. Kennedy)

E-mail: salman.durrani@anu.edu.au (S. Durrani)

E-mail: parastoo.sadeghi@anu.edu.au (P. Sadeghi)

E-mail: jason.mcewen@ucl.ac.uk (J. D. McEwen)

Subsequently, the SLSHT has been used to perform spatially varying spectral filtering [12], again with azimuthally symmetric window functions.

In obtaining the SLSHT distribution for spatio-spectral representation of a signal, the use of an azimuthally symmetric window function provides mathematical simplifications, however, such an approach cannot discriminate localized directional features in the spatio-spectral domain. This motivates the use of asymmetric window functions in the spatio-spectral transformation of a signal using the SLSHT. In order to serve this objective, we employ the definition of the localized spherical harmonic transform in [18] and define the SLSHT and the SLSHT distributions using azimuthally asymmetric window functions for spatial localization. Since the use of asymmetric window function enables the transform to reveal directional features in the spatio-spectral domain, we call the proposed transform the directional SLSHT. We also provide a harmonic analysis of the proposed transform and present an inversion relation to recover the signal from its directional SLSHT distribution.

Since the directional SLSHT distribution of a signal is required to be computed for each spatial position and for each spectral component, and data-sets on the sphere are of considerable size (e.g., three million samples on the sphere for current data-sets [37] and fifty million samples for forthcoming data-sets [38]), the evaluation of the directional SLSHT distribution is computationally challenging. We develop fast algorithms for this purpose. Through experimental results we show the numerical accuracy and efficient computation of the proposed directional SLSHT transform. Furthermore, due to the fact that the proposed directional SLSHT distribution depends on the window function used for spatial localization, we analyze the asymmetric band-limited window function with nominal concentration in an ellipsoidal region around the north pole, which is obtained from the Slepian concentration problem on the sphere. We also illustrate, through an example, the capability of the proposed directional SLSHT to reveal directional features in the spatio-spectral domain.

The remainder of the paper is structured as follows. In Section II, we review mathematical preliminaries related to the signals on the sphere, which are required in the sequel. We present the formulation of the directional SLSHT, its harmonic analysis and signal reconstruction from the SLSHT distribution in Section III. Different algorithms for the evaluation of the SLSHT distribution are provided in Section IV and the detailed analysis of the asymmetric window function is presented in Section V. In Section VI, we show timing and accuracy results of our algorithms and an illustration of the transform.

Concluding remarks are presented in Section VII.

## II. MATHEMATICAL BACKGROUND

In order to clarify the adopted notation, we review some mathematical background for signals defined on the sphere and the rotation group.

### A. Signals on the Sphere

In this work, we consider the square integrable complex functions  $f(\hat{\mathbf{x}})$  defined on unit sphere  $\mathbb{S}^2 \triangleq \{\mathbf{u} \in \mathbb{R}^3 : |\mathbf{u}| = 1\}$ , where  $|\cdot|$  denotes Euclidian norm,  $\hat{\mathbf{x}} \equiv \hat{\mathbf{x}}(\theta, \phi) \triangleq (\sin \theta \cos \phi, \sin \theta \sin \phi, \cos \theta)^T \in \mathbb{R}^3$  is a unit vector and parameterizes a point on the unit sphere with  $\theta \in [0, \pi]$  denoting the co-latitude and  $\phi \in [0, 2\pi)$  denoting the longitude. The inner product of two functions  $f$  and  $h$  on  $\mathbb{S}^2$  is defined as [39]

$$\langle f, h \rangle \triangleq \int_{\mathbb{S}^2} f(\hat{\mathbf{x}}) \overline{h(\hat{\mathbf{x}})} ds(\hat{\mathbf{x}}), \quad (1)$$

where  $\overline{(\cdot)}$  denotes the complex conjugate,  $ds(\hat{\mathbf{x}}) = \sin \theta d\theta d\phi$  and the integration is carried out over the unit sphere. With the inner product in (1), the space of square integrable complex valued functions on the sphere forms a complete Hilbert space  $L^2(\mathbb{S}^2)$ . Also, the inner product in (1) induces a norm  $\|f\| \triangleq \langle f, f \rangle^{1/2}$ . We refer the functions with finite induced norm as signals on the sphere.

The Hilbert space  $L^2(\mathbb{S}^2)$  is separable and the spherical harmonics form the archetype complete orthonormal set of basis functions. The spherical harmonics,  $Y_\ell^m(\hat{\mathbf{x}}) = Y_\ell^m(\theta, \phi)$ , for degree  $\ell \geq 0$  and order  $|m| \leq \ell$  are defined as [5], [36]

$$Y_\ell^m(\theta, \phi) = N_\ell^m P_\ell^m(\cos \theta) e^{im\phi}, \quad (2)$$

where

$$N_\ell^m = \sqrt{\frac{2\ell + 1}{4\pi} \frac{(\ell - m)!}{(\ell + m)!}} \quad (3)$$

denotes the normalization constant and  $P_\ell^m$  are the associated Legendre polynomials defined, for  $m \geq 0$ , by:

$$P_\ell^m(x) = \frac{(-1)^m}{2^\ell \ell!} \sqrt{(1-x^2)^m} \frac{d^{\ell+m}}{dx^{\ell+m}} (x^2 - 1)^\ell, \quad (4)$$

$$P_\ell^{-m}(x) = (-1)^m \frac{(\ell - m)!}{(\ell + m)!} P_\ell^m(x), \quad (5)$$

for  $|x| \leq 1$ . With the above definitions, the spherical harmonics form an orthonormal set of basis functions, i.e., they satisfy  $\langle Y_\ell^m, Y_{\ell'}^{m'} \rangle = \delta_{\ell\ell'} \delta_{mm'}$ , where  $\delta_{\ell\ell'}$  is the Kronecker delta.

By completeness and orthonormality of the spherical harmonics, we can expand any signal  $f \in L^2(\mathbb{S}^2)$  as

$$f(\hat{\mathbf{x}}) = \sum_{\ell=0}^{\infty} \sum_{m=-\ell}^{\ell} (f)_{\ell}^m Y_{\ell}^m(\hat{\mathbf{x}}), \quad (6)$$

where

$$(f)_{\ell}^m \triangleq \langle f, Y_{\ell}^m \rangle = \int_{\mathbb{S}^2} f(\hat{\mathbf{x}}) \overline{Y_{\ell}^m(\hat{\mathbf{x}})} ds(\hat{\mathbf{x}}) \quad (7)$$

denotes the spherical harmonic coefficient of degree  $\ell$  and order  $m$ . The signal  $f$  is said to be band-limited with maximum spherical harmonic degree  $L_f$  if  $(f)_{\ell}^m = 0, \forall \ell > L_f$ .

### B. Rotations on the Sphere and Wigner-D Functions

Rotations on the sphere are often parameterized using Euler angles  $(\alpha, \beta, \gamma) \in \text{SO}(3)$ , where  $\alpha \in [0, 2\pi)$ ,  $\beta \in [0, \pi]$  and  $\gamma \in [0, 2\pi)$  [36]. Using the ‘ $zyz$ ’ Euler convention, we define the rotation operator  $\mathcal{D}_{\rho}$ , for  $\rho = (\alpha, \beta, \gamma) \in \text{SO}(3)$ , which rotates a function on a sphere in the sequence of  $\gamma$  rotation around  $z$ -axis, then  $\beta$  rotation about  $y$ -axis followed by a  $\alpha$  rotation around  $z$ -axis. The spherical harmonic coefficient of a rotated signal  $\mathcal{D}_{\rho}f$  is related to the coefficients of the original signal by

$$(\mathcal{D}_{\rho}f)_{\ell}^m = \sum_{m'=-\ell}^{\ell} D_{m,m'}^{\ell}(\rho) (f)_{\ell}^{m'}, \quad \rho = (\alpha, \beta, \gamma), \quad (8)$$

where  $D_{m,m'}^{\ell}(\rho)$  denotes the Wigner- $D$  function [36] of degree  $\ell$  and orders  $m$  and  $m'$  and is given by

$$\begin{aligned} D_{m,m'}^{\ell}(\rho) &= D_{m,m'}^{\ell}(\alpha, \beta, \gamma) \\ &= e^{-im\alpha} d_{m,m'}^{\ell}(\beta) e^{-im'\gamma}, \quad \rho = (\alpha, \beta, \gamma), \end{aligned} \quad (9)$$

where  $d_{m,m'}^{\ell}(\beta)$  is the Wigner- $d$  function [36] and is defined as

$$\begin{aligned} d_{m,m'}^{\ell}(\beta) &= \sum_n (-1)^{n-m'+m} \\ &\times \frac{\sqrt{(\ell+m')!(\ell-m')!(\ell+m)!(\ell-m)!}}{(\ell+m'-n)!(n)!(\ell-n-m)!(n-m'+m)!} \\ &\times \cos\left(\frac{\beta}{2}\right)^{2\ell-2n+m'-m} \sin\left(\frac{\beta}{2}\right)^{2n-m'+m} \end{aligned} \quad (10)$$

### C. Signals on the Rotation Group $\text{SO}(3)$

For  $\ell \geq 0$  and  $m, m' \in \mathbb{Z}$  such that  $|m|, |m'| \leq \ell$ , the Wigner- $D$  functions in (9) form a complete set of orthogonal functions for the space  $L^2(\text{SO}(3))$  of

functions defined on the rotation group  $\text{SO}(3)$  and follow the orthogonality relation

$$\int_{\text{SO}(3)} D_{m,m'}^{\ell}(\rho) \overline{D_{q,q'}^p(\rho)} d\rho = \frac{8\pi^2}{2\ell+1} \delta_{\ell p} \delta_{mq} \delta_{m'q'}, \quad (11)$$

where  $d\rho = d\alpha \sin\beta d\beta d\gamma$  and the integral is a triple integral over all rotations  $(\alpha, \beta, \gamma) \in \text{SO}(3)$  [36]. Thus, any function  $f \in L^2(\text{SO}(3))$  may be expressed as

$$f(\rho) = \sum_{\ell=0}^{\infty} \sum_{m=-\ell}^{\ell} \sum_{m'=-\ell'}^{\ell'} (f)_{m,m'}^{\ell} D_{m,m'}^{\ell}(\rho), \quad (12)$$

where

$$(f)_{m,m'}^{\ell} = \frac{2\ell+1}{8\pi^2} \int_{\text{SO}(3)} f(\rho) \overline{D_{m,m'}^{\ell}(\rho)} d\rho. \quad (13)$$

The signal  $f$  is said to be band-limited with maximum degree  $L_f$  if  $(f)_{m,m'}^{\ell} = 0, \forall \ell > L_f$ .

### D. Discretization of $\mathbb{S}^2$ and $\text{SO}(3)$

In order to represent functions on  $\mathbb{S}^2$  and  $\text{SO}(3)$ , it is necessary to adopt appropriate tessellation schemes to discretize both the unit sphere domain and the Euler angle domain of  $\text{SO}(3)$ . We consider tessellation schemes that support a sampling theorem for band-limited functions, which is equivalent to supporting an exact quadrature.

For the unit sphere domain, we adopt the equiangular tessellation scheme [35] defined as  $\mathfrak{S}_L = \{\theta_{n_{\theta}} = \pi(2n_{\theta}+1)/(2L+1), \phi_{n_{\phi}} = 2\pi n_{\phi}/(2L+1) : 0 \leq n_{\theta} \leq L, 0 \leq n_{\phi} \leq 2L\}$ , which is a grid of  $(L+1) \times (2L+1)$  sample points on the sphere (including repeated samples of the south pole) that keeps the independence between  $\theta$  and  $\phi$  for fix value of  $\theta$ . For a band-limited function on the sphere  $f \in L^2(\mathbb{S}^2)$  with maximum spherical harmonic degree  $L_f$ , the sampling on the grid  $\mathfrak{S}_{L_f}$  ensures that all information of the function is captured in the finite set of samples and, moreover, that exact quadrature can be performed [35]. Note that this sampling theorem was developed only recently [35] and requires approximately half as many samples on the sphere as required by alternative equiangular sampling theorems on the sphere [34].

For the Euler angle representation of the rotation group  $\text{SO}(3)$ , we consider the equiangular tessellation scheme  $\mathfrak{E}_L = \{\alpha_{n_{\alpha}} = 2\pi n_{\alpha}/(2L+1), \beta_{n_{\beta}} = 2\pi n_{\beta}/(2L+1), \gamma_{n_{\gamma}} = 2\pi n_{\gamma}/(2L+1) : 0 \leq n_{\alpha}, n_{\gamma} \leq 2L, 0 \leq n_{\beta} \leq L\}$ . Again for a function  $f \in L^2(\text{SO}(3))$  with maximum spectral degree  $L_f$ , the sampling of a function  $f$  on  $\mathfrak{E}_{L_f}$  ensures that all information of the function is captured and also permits exact quadrature (which follows from the results developed on the sphere [35]).

### III. DIRECTIONAL SLSHT

We describe in this section the directional SLSHT, which is capable of revealing directional features of signals in the spatio-spectral domain. For spatial localization, we consider the band-limited azimuthally asymmetric window function which is spatially concentrated in some asymmetric region around the north pole. Since the rotation around the  $z$ -axis does not have any effect on an azimuthally symmetric function, the localized spherical harmonic transform using an azimuthally symmetric window function can be parameterized on the sphere. However, if an azimuthally asymmetric window is used to obtain localization in the spatial domain, the rotation of the window function is fully parameterized with the consideration of all three Euler angles  $(\alpha, \beta, \gamma) \in \text{SO}(3)$ . We refer to the spatially localized transform using an asymmetric window as the directional SLSHT. Here, we first define the directional SLSHT distribution which presents the signal in the spatio-spectral domain. Later in this section, we present the harmonic analysis of SLSHT distribution and provide an inversion relation to obtain the signal from its given directional SLSHT distribution.

#### A. Forward Directional SLSHT

*Definition 1 (Directional SLSHT):* For a signal  $f \in L^2(\mathbb{S}^2)$ , define the directional SLSHT distribution component  $g(\rho; \ell, m) \in L^2(\text{SO}(3))$  of degree  $\ell$  and order  $m$  as the spherical harmonic transform of a localized signal where localization is provided by the rotation operator  $\mathcal{D}_\rho$  acting on window function  $h \in L^2(\mathbb{S}^2)$ , i.e.,

$$g(\rho; \ell, m) \triangleq \int_{\mathbb{S}^2} f(\hat{\mathbf{x}}) (\mathcal{D}_\rho h)(\hat{\mathbf{x}}) \overline{Y_\ell^m(\hat{\mathbf{x}})} ds(\hat{\mathbf{x}}) \quad (14)$$

for  $0 \leq \ell \leq L_g$ ,  $|m| \leq \ell$ , where  $L_g = L_f + L_h$  denotes the maximum spherical harmonic degree for which the distribution components  $g(\rho; \ell, m)$  are non-zero, and  $L_f$  and  $L_h$  denote the band-limits of the signal  $f$  and the window function  $h$ , respectively. Also, each distribution component  $g(\rho; \ell, m)$  is band-limited in  $\rho = (\alpha, \beta, \gamma) \in \text{SO}(3)$  with maximum degree  $L_h$ , i.e., when expressed in terms of Wigner-D functions. We elaborate this shortly. Furthermore, we consider unit energy normalized window functions such that  $\langle h, h \rangle = 1$ .

*Remark 1:* The directional SLSHT distribution component in (14) can be interpreted as the spherical harmonic transform of the localized signal where the window function  $h$  provides asymmetric localization at spatial position  $\hat{\mathbf{x}} = \hat{\mathbf{x}}(\beta, \alpha) \in \mathbb{S}^2$  and the first rotation determines the orientation of the window function at  $\hat{\mathbf{x}}$ . If the window function is azimuthally symmetric, this orientation of the window function by  $\gamma$  becomes

invariant and the SLSHT distribution components are defined on  $L^2(\mathbb{S}^2)$  [10].

Since the maximum spectral degree for which the SLSHT distribution is defined is  $L_g = L_f + L_h$ , we consider the window function such that  $L_h \leq L_f$  to avoid extending  $L_g$  significantly above  $L_f$ . We discuss the localization of the window function in spatial and spectral domains later in the paper.

#### B. Harmonic Analysis

We now present the formulation of the directional SLSHT distribution if the signal  $f$  and the window function  $h$  are represented in the spectral domain. Using the expression of the spherical harmonics of a rotated function in (8), we can write the SLSHT distribution component  $g(\rho; \ell, m)$  in (14) as

$$g(\rho; \ell, m) = \sum_{\ell'=0}^{L_f} \sum_{m'=-\ell'}^{\ell'} (f)_{\ell'}^{m'} \quad (15)$$

$$\times \sum_{p=0}^{L_h} \sum_{q=-p}^p \sum_{q'=-p}^p (h)_p^{q'} D_{q,q'}^p(\rho) T(\ell', m'; p, q; \ell, m),$$

where

$$T(\ell', m'; p, q; \ell, m) = \int_{\mathbb{S}^2} Y_{\ell'}^{m'}(\hat{\mathbf{x}}) Y_p^q(\hat{\mathbf{x}}) \overline{Y_\ell^m(\hat{\mathbf{x}})} ds(\hat{\mathbf{x}}) \quad (16)$$

denotes the spherical harmonic triple product, which can be evaluated using Wigner-3j symbols or Clebsch-Gordan coefficients [36], [40].

*Remark 2:* By comparing  $g(\rho; \ell, m)$  in (15) with (12), we note that the band-limit of  $g(\rho; \ell, m)$  in  $\rho$  is given by  $L_h$ . Since  $\ell' \leq L_f$  and  $p \leq L_h$  in (15), our statement that the distribution component  $g(\rho; \ell, m)$  is non-zero for  $\ell \leq L_g = L_f + L_h$  follows since the triple product in (16) is non-zero for  $\ell \leq L_f + L_h$  only.

#### C. Inverse Directional SLSHT

Here, we define the inverse directional SLSHT to reconstruct a signal from its SLSHT distribution. The original signal can be reconstructed from its directional SLSHT distribution through the spectral domain marginal, that is, by integrating the SLSHT distribution components over the spatial domain  $\text{SO}(3)$  [18]. Using our harmonic formulation in (15), define  $(\hat{f})_\ell^m$  as the integral of the SLSHT distribution component  $g(\rho; \ell, m)$

over  $\text{SO}(3)$  giving

$$\begin{aligned}
(\hat{f})_\ell^m &= \int_{\text{SO}(3)} g(\rho; \ell, m) d\rho, \quad 0 \leq \ell \leq L_f \\
&= \sum_{\ell'=0}^{L_h} \sum_{m'=-\ell'}^{\ell'} (f)_{\ell'}^{m'} \sum_{p=0}^{L_h} \sum_{q=-p}^p \sum_{q'=-p}^p (h)_p^{q'} \\
&\quad \times T(\ell', m'; p, q; \ell, m) \int_{\text{SO}(3)} D_{q,q'}^p(\rho) d\rho \\
&= \sqrt{16\pi^3} (h)_0^0 (f)_\ell^m, \tag{17}
\end{aligned}$$

where we have used the following property of Wigner- $D$  functions

$$\int_{\text{SO}(3)} D_{q,q'}^p(\rho) d\rho = 8\pi^2 \delta_{p0} \delta_{q0} \delta_{q'0}, \tag{18}$$

which stems from (11). Using the expression in (17), we can find the spherical harmonic coefficient  $(f)_\ell^m$  of the signal  $f$  as

$$(f)_\ell^m = \frac{(\hat{f})_\ell^m}{\sqrt{16\pi^3} (h)_0^0}, \tag{19}$$

which indicates that we only need to know the DC component of the window function  $(h)_0^0$  in order to obtain the signal from its directional SLSHT distribution. It further imposes the condition that the DC component of the window function must be non-zero. Although the distribution components in (15) are defined up to degree  $L_g = L_f + L_h$ , we only require the components up to  $L_f$  for signal reconstruction.

Since the directional SLSHT distribution components  $g(\rho; \ell, m)$  in (14) are defined for  $\ell \leq L_g$ , the number of distribution components are of the order  $L_g^2$ , while the sampling of  $\rho$  is of the order  $L_h^3$ ; thus, the direct evaluation of the directional SLSHT distribution is prohibitively computationally expensive. Therefore efficient algorithms need to be developed which reduce the computational complexity. We address this problem in the next section.

#### IV. EFFICIENT COMPUTATION OF DIRECTIONAL SLSHT DISTRIBUTION

Here, we present efficient algorithms for the computation of the directional SLSHT distribution of a signal and the signal reconstruction from its directional SLSHT distribution. First, we discuss the computational complexities if the SLSHT distribution components are computed using direct quadrature as given in (14) or using the harmonic formulation in (15). Later, we develop an alternative harmonic formulation which reduces the computational burden. Finally, we present an efficient

algorithm that incorporates a factoring of rotations [41] and exploits the FFT.

First we need to parameterize the required tessellation schemes for  $\mathbb{S}^2$  for the representation of the signal  $f$  and the window  $h$  and for  $\text{SO}(3)$  which forms the spatial domain of the directional SLSHT distribution. Since the maximum spectral degree of the signal  $f$  is  $L_f$ , we therefore consider the equiangular tessellation  $\mathfrak{E}_{L_f}$  to represent signals on  $L^2(\mathbb{S}^2)$ . Since the maximum degree for all SLSHT distribution components  $g(\rho; \ell, m)$  in  $\rho$  is  $L_h$ , we therefore consider the tessellation  $\mathfrak{E}_{L_h}$  to represent the SLSHT distribution components on  $L^2(\text{SO}(3))$ .

##### A. Direct Quadrature and Harmonic Formulation

We define the forward spatio-spectral transform as evaluation of each SLSHT distribution component  $g(\rho; \ell, m)$ . Evaluation of the forward spatio-spectral transform using exact quadrature in (14) requires the computation of two dimensional summation over the tessellation of  $\mathbb{S}^2$  for each 3-tuple  $(\alpha, \beta, \gamma)$ . Since there are  $O(L_h^3)$  such 3-tuples in the tessellation scheme  $\mathfrak{E}_{L_h}$  and the SLSHT distribution components are of the order  $O(L_f^2)$ , the computational complexity to compute all distribution components using direct quadrature is  $O(L_f^4 L_h^3)$ . Using the harmonic formulation in (15), the complexity to compute each SLSHT distribution component is  $O(L_f^2 L_h^6)$  and to compute all SLSHT distribution components is  $O(L_f^4 L_h^6)$ . Although the harmonic formulation in (15) is useful to establish that the signal can be reconstructed from the directional SLSHT distribution, it is much more computationally demanding than direct quadrature. We develop efficient algorithms in the next subsection which improve the computational complexity of the harmonic formulation and make it more efficient than direct quadrature.

For the inverse directional SLSHT distribution, we only need to integrate over  $\text{SO}(3)$  to obtain the signal in the spherical harmonic domain as proposed in (17). Since the integral can be evaluated by a summation over all Euler angles using quadrature weights, an efficient way to recover the signal from its SLSHT distribution is through direct quadrature, with complexity of  $O(L_h^3)$  for each distribution component and  $O(L_f^2 L_h^3)$  for all components.

1) *Exact Quadrature and Quadrature Weights:* In order to evaluate the integral in (17) exactly, we need to define quadrature weights along Euler angle  $\beta$  in the tessellation  $\mathfrak{E}_{L_h}$ . We evaluate the integral in (17) by the

following summation

$$(\hat{f})_\ell^m = \frac{1}{(2L_h + 1)^3} \sum_{n_\alpha=0}^{2L_h} \sum_{n_\beta=0}^{L_h} \sum_{n_\gamma=0}^{2L_h} \times g(\alpha_{n_\alpha}, \beta_{n_\beta}, \gamma_{n_\gamma}; \ell, m) q(\beta_{n_\beta}), \quad (20)$$

where the quadrature weights  $q(\beta_{n_\beta})$  are evaluated by employing the method outlined in [35], giving

$$q(\beta_{n_\beta}) = \begin{cases} 4\pi^2 \left( \lfloor \frac{L_h}{2} \rfloor + \frac{1}{2} \right)^{-1}, & \beta_{n_\beta} = 0 \\ 8\pi^2 \sum_{m=-L_h}^{L_h} w(-m) \cos m\beta_{n_\beta}, & \text{otherwise} \end{cases} \quad (21)$$

where  $w(m)$  is defined as [35]

$$w(m) = \begin{cases} \frac{\pm i\pi}{2}, & m = \pm 1, \\ 0, & m \text{ odd}, m \neq 1, \\ \frac{2}{1-m^2}, & m \text{ even}. \end{cases} \quad (22)$$

### B. Forward Directional SLSHT: Semi-Fast Algorithm

We consider an alternative harmonic formulation in order to reduce the computational complexity of the forward SLSHT. We may write the directional SLSHT distribution component  $g(\rho; \ell, m)$  in (14) as a spherical convolution [15] of  $h$  and the spherical harmonic modulated signal  $\bar{f}Y_\ell^m$ , giving

$$g(\rho; \ell, m) = \sum_{p=0}^{L_h} \sum_{q=-p}^p \sum_{q'=-p}^p \overline{(\bar{f}Y_\ell^m)_p^q} (h)_p^{q'} D_{q,q'}^p(\alpha, \beta, \gamma), \quad (23)$$

which can be expressed, using the definition of the Wigner-D function in (9), as

$$g(\rho; \ell, m) = \sum_{p=0}^{L_h} \sum_{q=-p}^p \sum_{q'=-p}^p \overline{(\bar{f}Y_\ell^m)_p^q} \times (h)_p^{q'} d_{q,q'}^p(\beta) e^{-iq'\gamma} e^{-iq\alpha}. \quad (24)$$

The band-limit of the spherical harmonic modulated signal  $\bar{f}Y_\ell^m$  is  $L_f + \ell$ . Since the maximum  $\ell$  for which  $g$  is non-zero is  $L_f + L_h$ , we must compute up to  $\bar{f}Y_{L_f+L_h}^m$ , which is band-limited to  $2L_f + L_h$ . However, we *only* need to compute the spherical harmonic coefficients  $(\bar{f}Y_\ell^m)_p^q$  of the modulated signal up to degree  $p \leq L_h$ . Therefore, the computation of spherical harmonic transform of  $\bar{f}Y_\ell^m$  is an interesting sub-problem. By either using the separation of variable approach or the method outlined in [35], the spherical harmonic coefficients  $(\bar{f}Y_\ell^m)_p^q$  for  $0 \leq p \leq L_h$ ,  $|q| \leq p$  of the signal  $\bar{f}Y_\ell^m$  can be computed in  $O(L_f^2 \min(\log_2 L_f, L_h))$  time for a given  $\ell$  and  $m$  (see Appendix A for details).

Using the spherical harmonic transform method in [35],  $(h)_p^{q'}$  can be computed in  $O(L_h^3)$ . The product inside the inner summation of (24) can be computed in  $O(L_h^2)$  for each  $p$  and for all  $|q|, |q'| \leq p$ . The inner two summations of (24) include complex exponentials and therefore we can employ an FFT to evaluate these two summations in  $O(L_h^2 \log_2 L_h)$  for each  $p$  and each  $\beta$ . Since, both  $p$  and  $\beta$  are of the order  $L_h$ , each SLSHT distribution component can be computed using (24) in  $O(L_f^2 \min(\log_2 L_f, L_h) + L_h^4 \log_2 L_h)$  and all components can be computed with overall complexity of  $O(L_f^4 \min(\log_2 L_f, L_h) + L_f^2 L_h^4 \log_2 L_h)$ . It is important to note that we have considered the factor  $L_f^4 \min(\log_2 L_f, L_h)$ , which arises from the computation of the spherical harmonic coefficients of  $\bar{f}Y_\ell^m$ , in the total complexity and this may dominate the other factor  $L_f^2 L_h^4 \log_2 L_h$  if  $L_h \ll L_f$ . In any case, the alternative harmonic formulation in (24) is more efficient to compute than the harmonic formulation in (15) or direct quadrature of (14).

Using the factoring of rotations approach which was first proposed in [41] and has been used in the implementations of the fast spherical convolution [42] and the directional spherical wavelet transform [15], the complexity of the harmonic formulation in (24) can be reduced further. We present this development in the next subsection.

### C. Forward Directional SLSHT: Fast Algorithm

Here we employ a factoring of rotations to develop an algorithm which reduces the factor  $L_f^2 L_h^4 \log_2 L_h$  in the complexity of the semi-fast case and thus improves the performance of the overall algorithm. It also reduces the asymptotic complexity of the overall algorithm when  $O(L_f^2 L_h^4 \log_2 L_h)$  dominates in the overall computational complexity of the formulation in (24), i.e., when  $L_h^4 \log_2 L_h > L_f^2 \min(\log_2 L_f, L_h)$ .

By factoring the single rotation by  $(\alpha, \beta, \gamma)$  into two rotations [15], [41], [42]

$$\begin{aligned} \mathcal{D}_\rho &= \mathcal{D}_{\rho_1} \mathcal{D}_{\rho_2}, \quad \rho = (\alpha, \beta, \gamma), \\ \rho_1 &= (\alpha - \pi/2, -\pi/2, \beta), \quad \rho_2 = (0, \pi/2, \gamma + \pi/2), \end{aligned} \quad (25)$$

and noting the effect of rotation on spherical harmonic coefficients in (8), we can write the Wigner-D function in (9) as

$$D_{q,q'}^p(\alpha, \beta, \gamma) = i^{q-q'} \sum_{q''=-p}^p \Delta_{q''q}^p \Delta_{q''q'}^p e^{-iq\alpha - iq''\beta - iq'\gamma}, \quad (26)$$

where  $\Delta_{qq'}^p = d_{q,q'}^p(\pi/2)$  and we have used the following symmetry properties of Wigner- $d$  functions [40]

$$\begin{aligned} d_{q,q'}^p(\beta) &= (-1)^{q-q'} d_{q,q'}^p(-\beta) = (-1)^{q-q'} d_{-q,-q'}^p(\beta) \\ &= (-1)^{q-q'} d_{q',q}^p(\beta) = d_{-q',-q}^p(\beta). \end{aligned} \quad (27)$$

Using the Wigner- $D$  expansion given in (26), we can write the alternative harmonic formulation of the SLSHT distribution component  $g(\rho; \ell, m)$  in (23) as

$$\begin{aligned} g(\rho; \ell, m) &= \sum_{p=0}^{L_h} \sum_{q=-p}^p \sum_{q'=-p}^p \overline{(fY_\ell^m)_p^q(h)}_p^{q'} i^{q-q'} \\ &\times \sum_{q''=-p}^p \Delta_{q''q}^p \Delta_{q''q'}^p e^{-iq\alpha - iq''\beta - q'\gamma}, \end{aligned} \quad (28)$$

where  $\rho = (\alpha, \beta, \gamma)$ . By reordering the summations we can write

$$\begin{aligned} g(\rho; \ell, m) &= \sum_{q=-L_h}^{L_h} \sum_{q'=-L_h}^{L_h} \sum_{q''=-L_h}^{L_h} C_{q,q',q''}(\ell, m) \\ &\times e^{-iq\alpha - iq''\beta - q'\gamma}, \quad \rho = (\alpha, \beta, \gamma), \end{aligned} \quad (29)$$

where

$$C_{q,q',q''}(\ell, m) = i^{q-q'} \sum_{p=\max(|q|, |q'|, |q''|)}^{L_h} \Delta_{q''q}^p \Delta_{q''q'}^p \overline{(fY_\ell^m)_p^q(h)}_p^{q'}. \quad (30)$$

Comparatively, the computation of the SLSHT distribution components using the expression given by (29) is not more efficient than the initial expression (24). However, the presence of complex exponentials can be exploited by employing FFTs to evaluate the involved summations.

*1) Efficient Implementation:* The objective of factoring the rotations is to carry out the  $\beta$  rotation along the  $y$ -axis as a rotation along the  $z$ -axis. The rotations along the  $z$ -axis are parameterized using complex exponentials and thus these rotations can be applied with much less computational burden, by exploiting the power of an FFT, relative to a rotation about the  $y$ -axis. All the three rotations which characterize the spatial domain of the SLSHT distribution components appear in complex exponentials in (29) and thus we can use FFTs to evaluate the summation of  $C_{q,q',q''}(\ell, m)$  over  $q, q'$  and  $q''$ . First we need to compute  $C_{q,q',q''}(\ell, m)$  for each  $\ell$  and for each  $m$  which requires the one-dimensional summation over three dimensional grid formed by  $q, q'$  and  $q''$  and thus can be computed in  $O(L_h^4)$ . Using  $C_{q,q',q''}(\ell, m)$ , the summation over the complex exponentials in (29) can be carried out in  $O(L_h^3 \log_2 L_h)$  using FFTs. The overall complexity of this approach is dominated by the computation of  $C_{q,q',q''}(\ell, m)$ , that is,  $O(L_h^4)$  for each SLSHT distribution component and  $O(L_f^2 L_h^4)$  for the

complete SLSHT distribution. We note that the evaluation of  $C_{q,q',q''}(\ell, m)$  requires the computation of  $\Delta_{qq'}^p$  which can be evaluated over the  $(q, q')$  plane for each  $p$  using the recursion formula of [43] with a complexity of  $O(L_h^2)$ . Since  $p$  is of the order  $L_h$ , the  $\Delta$  matrices can be evaluated in  $O(L_h^3)$ , which does not change the overall complexity of our proposed algorithm. The overall asymptotic complexity of our fast algorithm is thus  $O(L_f^4 \min(\log_2 L_f, L_h) + L_f^2 L_h^4)$ .

*Remark 3:* If we want to analyze the signal  $f$  with multiple window functions, then we do not need to recalculate the spherical harmonic transform of the modulated signal  $\bar{f} Y_\ell^m$ , which accounts for the  $O(L_f^2 \min(\log_2 L_f, L_h))$  factor in the overall complexity. Once it is computed, the SLSHT distribution can be computed in  $O(L_f^2 L_h^4)$  time for each window function of the same band-limit using the proposed efficient implementation.

Our proposed formulation and efficient implementation can be further optimized in the case of a steerable window function. Steerable functions have an azimuthal harmonic band-limit in  $m$  that is less than the band-limit in  $\ell$  (see [20] for further details about steerability on the sphere). In this case, the  $L_f^2 L_h^4$  factor contributing to the overall asymptotic complexity of the fast algorithm is reduced to  $L_f^2 L_h^3$ . Furthermore, we may then compute the directional SLSHT for any continuous  $\gamma \in [0, 2\pi)$  from a small number of basis orientations (due to the linearity of the SLSHT).

If the signal and window function are real, the computational time can be further reduced by considering the conjugate symmetry relation of the spherical harmonic coefficients. Furthermore, in this setting, the SLSHT distribution components also satisfy the conjugate symmetry property

$$g(\rho; \ell, -m) = (-1)^m \overline{g(\rho; \ell, m)} \quad (31)$$

and we do not need to compute the SLSHT distribution components of negative orders.

## V. WINDOW LOCALIZATION IN SPATIAL AND SPECTRAL DOMAINS

The directional SLSHT distribution is the spherical harmonic transform of the product of two functions, the signal  $f$  and the rotated window function  $h$  and we must be careful in interpreting the directional SLSHT distribution in the sense that we do not mistake using the signal to study the window because there is no distinction mathematically. The window function should be chosen such that it provides spatial localization in some spatial region around the north pole (origin). Since

we have considered a band-limited window function, the window function cannot be perfectly localized in the spatial domain due to the uncertainty principle on the sphere [44]. However, it can be optimally localized by maximizing the energy concentration of the window function in the desired directional region [2].

The interpretation and the effectiveness of the directional SLSHT distribution depends on the chosen window function. The window function with maximum localization in some defined asymmetric region provides directional localization and thus reveals directional features in the spatio-spectral domain. The more directional the window function, the more directional features it can reveal in the spatio-spectral domain but the larger the maximum spherical harmonic degree  $L_h$ . Recall that the maximum degree of the directional SLSHT distribution components is given by  $L_g = L_f + L_h$ . Thus, when the signal is expressed in the spatio-spectral domain its spectral domain is extended by  $L_h$ , which results in spectral leakage. Therefore, we want the window function to be simultaneously maximally localized in some spatial region  $\mathcal{R} \subset \mathbb{S}^2$  and have the minimum possible band-limit which achieves the desired level of energy concentration in the spatial region  $\mathcal{R}$ . This problem is well known in time-frequency analysis [45] and has been extended to spatio-spectral analysis on the sphere for azimuthally symmetric window functions [10], where the minimum band-limit azimuthally symmetric eigenfunction obtained from the Slepian concentration problem on the sphere [2], [32] has been proposed as a suitable window function [10].

Here, we propose using a band-limited eigenfunction obtained from the solution of the Slepian concentration problem [2] as a window function, concentrated in a spatially localized ellipsoidal region around the north pole. We first parameterize the ellipsoidal region and later analyze the resulting eigenfunctions from the perspective of the uncertainty principle on the sphere [44]. We note that the choice of the asymmetric region as an ellipsoidal region is only one possibility and the analysis can be extended to other asymmetric regions such as strip regions around the north pole [46].

#### A. Parametrization of Window Function

We consider a band-limited window function of maximum spherical harmonic degree  $L_h$ , which is spatially concentrated in the asymmetric ellipsoidal region on the sphere with major axis along the  $x$ -axis, and thus is orientated along the  $x$ -axis. The ellipsoidal region can be parameterized using the focus  $\theta_c$  of the ellipse along the positive  $x$ -axis and the arc length  $a$  of the semi-major

axis:

$$\mathcal{R}_{(\theta_c, a)} \triangleq \{(\theta, \phi) : \Delta_s((\theta, \phi), (\theta_c, 0)) + \Delta_s((\theta, \phi), (\theta_c, \pi)) \leq 2a\}, \quad (32)$$

where  $0 \leq \theta_c \leq \pi/2$  and  $\theta_c \leq a \leq \pi/2$ . Here  $\Delta_s((\theta, \phi), (\theta', \phi')) = \arccos(\sin \theta \sin \theta' \cos(\phi - \phi') + \cos \theta \cos \theta')$  denotes the angular distance between two points  $(\theta, \phi)$  and  $(\theta', \phi')$  on the sphere.

*Remark 4:* For a given focus  $\theta_c$ , the region becomes more directional as the arc length  $a$  approaches  $\theta_c$ . For  $a = \pi/2$ , the region becomes azimuthally symmetric, i.e., we recover the polar cap of central angle  $\pi/2$ .

As an illustration, the ellipsoidal regions  $\mathcal{R}_{(\theta_c, a)}$  with focus  $\theta_c = \pi/6$  and  $a \in \{\pi/6 + \pi/240, \pi/6 + \pi/120, \pi/6 + \pi/80\}$  are shown in Fig. 1.

#### B. Slepian Concentration Problem

As a result of the Slepian concentration problem [2], [46] to find the band-limited function with bandwidth  $L_h$  and maximal spatial concentration in an ellipsoidal region  $\mathcal{R}_{(\theta_c, a)}$ , we obtain  $(L_h + 1)^2$  eigenfunctions. The eigenvalue associated with each eigenfunction serves as a measure of the energy concentration in the spatial region. Here we consider the use of the band-limited eigenfunction with maximum energy concentration in the ellipsoidal region for given band-limit  $L_h$  and refer to such an eigenfunction as the eigenfunction window. If  $A$  denotes the area of the ellipsoidal region, it is shown [2], [46] that most of the eigenvalues lie either near zero or unity for both symmetric and asymmetric regions and the sum of all eigenvalues, referred as an equivalent of the Shannon number [2], is equal to  $N_0 = A(L_h + 1)^2 / (4\pi)$ . Also, it is shown empirically in [32] that there exist less than or equal to  $N_0 - 1$  spatially concentrated eigenfunctions with non-insignificant energy concentration. By noting these developments and empirical results, and considering that  $L_h$  must be chosen that we obtain at least one eigenfunction which is spatially concentrated in the ellipsoidal region, we recover the following empirical lower bound for  $L_h$ :

$$L_h \gtrsim B_h = 2 \left\lceil \sqrt{\frac{2\pi}{A}} \right\rceil - 1, \quad A = \int_{\mathcal{R}_{(\theta_c, a)}} ds(\hat{\mathbf{x}}), \quad (33)$$

where  $\lceil (\cdot) \rceil$  denotes the integer ceiling function (this bound follows directly from  $N_0 \gtrsim 2$ ). We analyze this bound later in this section.

Let  $\lambda_{\max}$  denote the eigenvalue associated with the most spatially concentrated eigenfunction. By finding the minimum value of  $L_h$  which ensures that  $\lambda_{\max}$  is



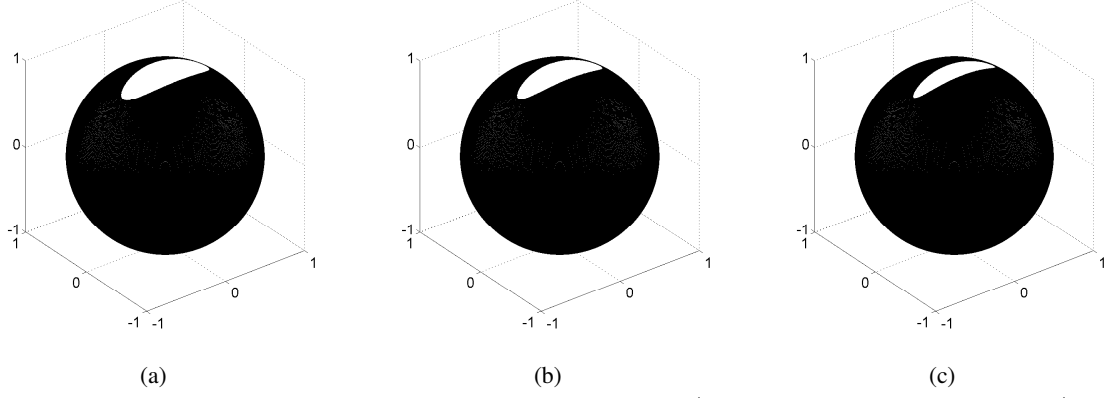


Fig. 1: Ellipsoidal regions  $\mathcal{R}_{(\theta_c, a)}$  on the sphere with focus  $\theta_c = \pi/6$  and major axis: (a)  $a = \pi/6 + \pi/80$ , (b)  $a = \pi/6 + \pi/120$  and (c)  $a = \pi/6 + \pi/240$ .

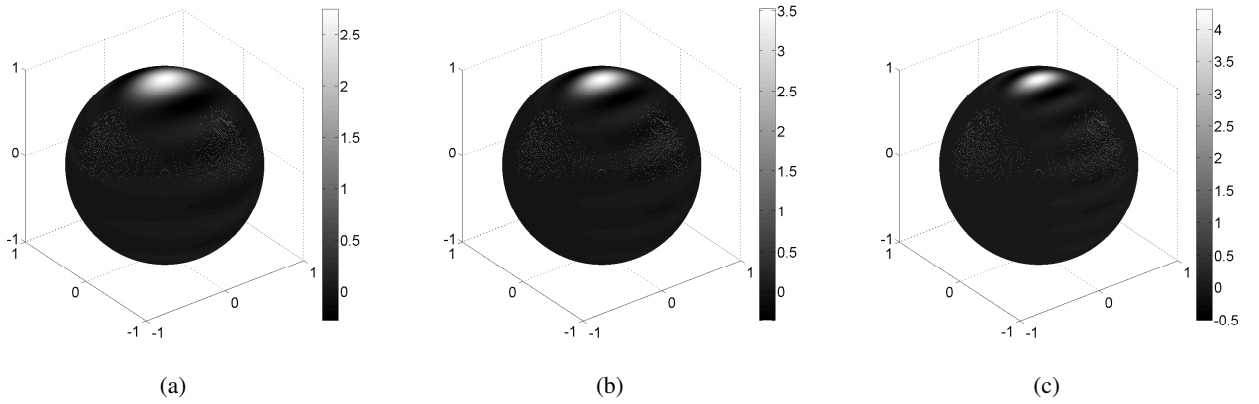


Fig. 2: Band-limited eigenfunction windows  $h$  obtained from Slepian concentration problem on the sphere with maximal spatial concentration in an ellipsoidal region  $\mathcal{R}_{(\theta_c, a)}$  of focus  $\theta_c = \pi/6$  and major axis: (a)  $a = \pi/6 + \pi/80$ , (b)  $a = \pi/6 + \pi/120$  and (c)  $a = \pi/6 + \pi/240$ .

greater than or equal to the desired energy concentration, an eigenfunction window  $h(\hat{x})$  with desired energy concentration in the ellipsoidal region and minimum possible band-limit  $L_h$  can be obtained. Thus, the focus of an ellipsoidal region  $\theta_c$ , arc length of semi-major axis  $a$  and maximum spectral degree  $L_h$  fully parameterize the eigenfunction window. As an illustration, the three eigenfunction windows having 90% spatial concentration in the ellipsoidal regions  $\mathcal{R}_{(\theta_c, a)}$  with focus  $\theta_c = \pi/6$  and  $a \in \{\pi/6 + \pi/240, \pi/6 + \pi/120, \pi/6 + \pi/80\}$  and respective maximum spherical harmonic degree  $L_h \in \{18, 14, 11\}$  are shown in Fig. 2. For these ellipsoidal regions, in Fig. 3 we show  $\lambda_{\max}$  versus spherical harmonic band-limit  $L$  denoting the band-limit of the most concentrated eigenfunction window, where we note the difference in  $L_h$  and the bound  $B_h$  for the desired concentration level. For 90% desired concentration level, we observe that the spherical harmonic degree  $L_h$  which ensures  $\lambda_{\max} \geq 0.9$  deviates further from the bound

$B_h$  given by (33) as the concentration region becomes more directional (as expected since the bound does not incorporate the level of directionality of the region).

### C. Analysis of Eigenfunction Window Concentrated in Ellipsoidal Region

1) *Directionality*: For the use of the eigenfunction window in obtaining the directional SLSHT distribution, the directionality of the eigenfunction window must be a key criterion in selecting the eigenfunction window for the identification of localized features of a signal in the spatio-spectral domain. Also, the directionality of the eigenfunction window depends on the directionality of the ellipsoidal region. We use the definition of the auto-correlation function on the sphere as a measure of the directionality of the eigenfunction window [20]. Since the major axis and minor axis of an ellipsoidal region lie along  $x$ -axis and  $y$ -axis respectively, the auto-correlation

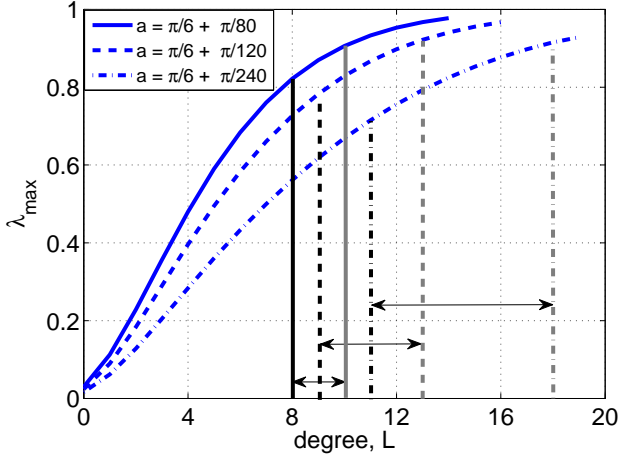


Fig. 3: The maximum eigenvalue  $\lambda_{\max}$  of the eigenfunction  $h$  with spherical harmonic band-limit  $L$  for spatial concentration in an ellipsoidal region of focus  $\theta_c = \pi/6$  and major axis  $a$  as indicated. Black vertical lines indicate the bound on the band-limit  $B_h$  given by (33) and the gray vertical lines indicate the actual  $L_h$  which ensures 90% concentration in an ellipsoidal region.

function is defined as the inner product of eigenfunction window with its version rotated around the  $z$ -axis:

$$C_h(\varsigma) = \langle D_{\rho_1} h, h \rangle, \quad \rho_1 = (0, 0, \varsigma), \quad \varsigma \in [0, \frac{\pi}{2}], \quad (34)$$

which can be expressed in the harmonic domain as

$$C_h(\varsigma) = \sum_{\ell=0}^{L_h} \sum_{m=-\ell}^{\ell} e^{im\varsigma} |h_{\ell}^m|^2. \quad (35)$$

Due to the symmetry of the ellipsoidal region and the eigenfunction window, we have considered  $\varsigma$  in the range of 0 to  $\pi/2$ .

For the eigenfunction windows presented in the previous subsection, the auto-correlation function for each window is shown in Fig. 4, which indicates that  $C_h(\varsigma)$  decays more rapidly from unity at  $\varsigma = 0$  for more directional window and therefore, the peakedness of  $C_h(\varsigma)$  quantifies the ability of the window function to reveal the localized directional features of a signal in the spatio-spectral domain.

2) *Spatial and Spectral Localization*: Here we study the spatial and spectral localization of eigenfunction windows from the perspective of the uncertainty principle on the sphere [44], [47], according to which, the function cannot be simultaneously localized in both the spatial and spectral domains. The following inequality specifies the uncertainty principle for unit energy functions defined on the sphere, which relates the trade-off between

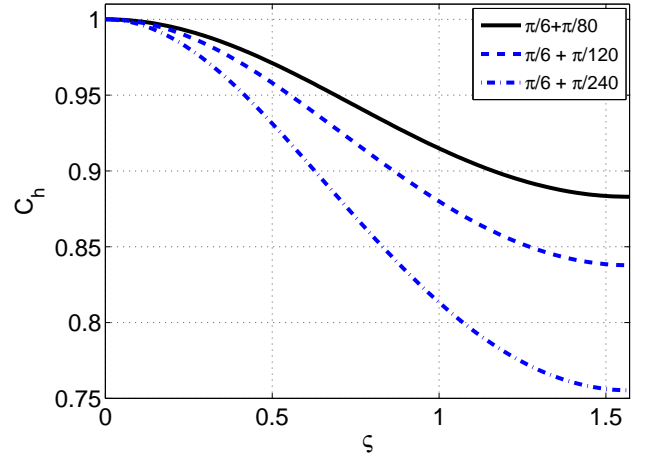


Fig. 4: Auto-correlation function  $C_h(\varsigma)$  as described in (34) for eigenfunction windows  $h$  with spatial concentration in an ellipsoidal region of focus  $\theta_c = \pi/6$  and major axis  $a$  as indicated.

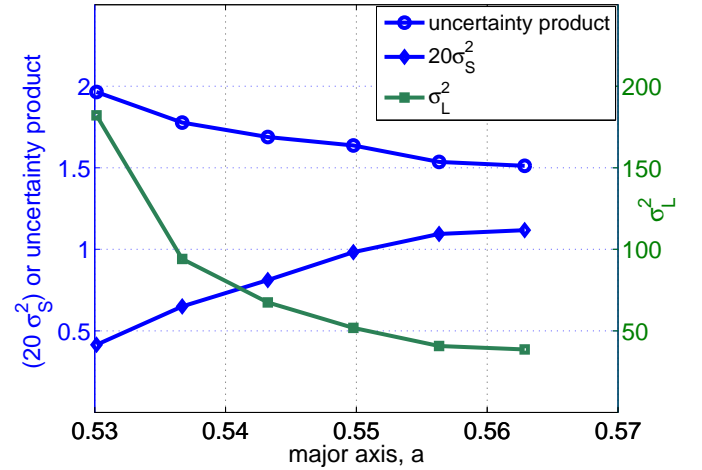


Fig. 5: Spatial variance ( $20\sigma_S^2$ ), spectral variance ( $\sigma_L^2$ ) and uncertainty product, as described in (36), (37) and (38), are shown for eigenfunctions with spatial concentration in an ellipsoidal region of focus  $\theta_c = \pi/6$  and major axis  $a$  as indicated. We have plotted a scaled value of spatial variance ( $20\sigma_S^2$ ) for better visualization.

the spatial and spectral localization of a function:

$$\frac{\sigma_S}{\sqrt{1 - \sigma_S^2}} \cdot \sigma_L \geq 1, \quad (36)$$

where  $\sigma_S$  and  $\sigma_L$  denote the variance of the band-limited unit energy eigenfunction window in the spatial domain and spectral domain respectively and are defined as [47]

$$\sigma_S^2 = 1 - \left( \frac{1}{2} \int_{\mathbb{S}^2} \sin(2\theta) |h(\theta, \phi)|^2 d\theta d\phi \right)^2 \quad (37)$$

and

$$\sigma_L^2 = \sum_{\ell=0}^{L_h} \ell(\ell+1) \sum_{m=-\ell}^{\ell} |h_{\ell}^m|^2. \quad (38)$$

Due to the consideration of unit energy functions,  $0 \leq \sigma_S \leq 1$ . We note that smaller variance indicates better localization of the window function. The variance in the spatial and spectral domains and the uncertainty product for eigenfunctions concentrated in an ellipsoidal region of focus  $\pi/6$  and major-axis of different values are shown in Fig. 5. As expected, the variance in the spatial domain decreases as the region becomes more directional, whereas the variance in the spectral domain increases because  $L_h$  increases. We also note that the uncertainty product increases as the region becomes more directional.

## VI. RESULTS

In this section, we first demonstrate the numerical validation and computation time of our algorithms to evaluate the directional SLSHT components. Later, we provide an example to illustrate the capability of the directional SLSHT, showing that it reveals the directional features of signals in the spatio-spectral domain. The implementation of the our algorithms is carried out in MATLAB, using the MATLAB interface of the SSHT<sup>1</sup> package (the core algorithms of which are written in C and which also uses the FFTW<sup>2</sup> package to compute Fourier transforms) to efficiently compute forward and inverse spherical harmonic transforms [35].

### A. Numerical Validation and Computation Time

In order to evaluate the numerical accuracy and the computation time, we carry out the following numerical experiment. We use the band-limited function  $h$  for spatial localization with band-limit  $L_h = 18$  and spatial localization in the region  $\mathcal{R}_{(\pi/6, \pi/6 + \pi/240)}$ . We generate band-limited test signals with band-limits  $18 \leq L_f \leq 120$  by generating spherical harmonic coefficients with real and imaginary parts uniformly distributed in the interval  $[0, 1]$ .

For the given test signal, we measure the computation time  $\tau_1$  to compute all directional SLSHT distribution components  $g(\rho; \ell, m)$  for  $\ell \leq L_f + L_h$  and  $m \leq |\ell|$  using our fast algorithm presented in Section IV-C, where we compute the Wigner- $d$  functions on-the-fly for the argument  $\pi/2$  by using the recursion of Trapani [43]. We also record the time  $\tau_2$  to compute the

spherical harmonic transform of the modulated signal only and the time  $\tau_3$  to recover a signal from its SLSHT distribution components. For the computation of the spherical harmonic transform of the modulated signal, we use the separation of variable approach presented in Appendix A. All numerical experiments are performed using MATLAB running on a 2.4 GHz Intel Xeon processor with 64 GB of RAM and the results are averaged over ten test signals. The computation time  $\tau_1$  and  $\tau_2$  in seconds are plotted against the band-limit  $L_f$  of the test signal in Fig. 6a, which scale as  $O(L_f^4)$  and thus corroborates the theoretical complexity. We also note that the major cost in the evaluation of SLSHT distribution components is the computation of the spherical harmonic transform of the spherical harmonic modulated signal. The computation time  $\tau_3$  for the inverse directional SLSHT is plotted in Fig. 6b, which evolves as  $O(L_f^2)$  for fixed  $L_h$ , again corroborating the theoretical complexity.

We reconstruct the original signal from its SLSHT distribution components using (20) and (17), in order to assess the numerical accuracy of our algorithms by measuring the maximum absolute error between the original spherical harmonic coefficients of the test signal and the reconstructed values. The maximum absolute error is plotted in Fig. 6c for different band-limits  $L_f$ , which illustrates that our algorithms achieve very good numerical accuracy with numerical errors at the level of floating point precision.

### B. Directional SLSHT Illustration

In order to illustrate the capability of the proposed transform to reveal the localized contribution of spectral contents and probe the directional features in the spatio-spectral domain, we analyze the Mars topographic map (height above geoid) as a signal on the sphere, which is obtained by using the spherical harmonic model of the topography of Mars<sup>3</sup>. The Mars topographic map is shown in Fig. 7 in the spatial domain, where the grand canyon Valles Marineris and the mountainous regions of Tharsis Montes and Olympus Montes are shown, leading to the high frequency contents. We note that the mountainous regions are non-directional features of the Mars map, whereas the grand canyon serves as a directional feature with direction orientated along a line of approximate constant latitude. The spherical harmonic coefficients certainly provide details about the presence of higher degree spherical harmonics in the signal, but do not reveal any information about the localized contribution of higher degree spherical harmonics.

<sup>1</sup><http://www.jasonmcewen.org/>

<sup>2</sup><http://www.fftw.org/>

<sup>3</sup><http://www.ipgp.fr/~wieczor/SH/>

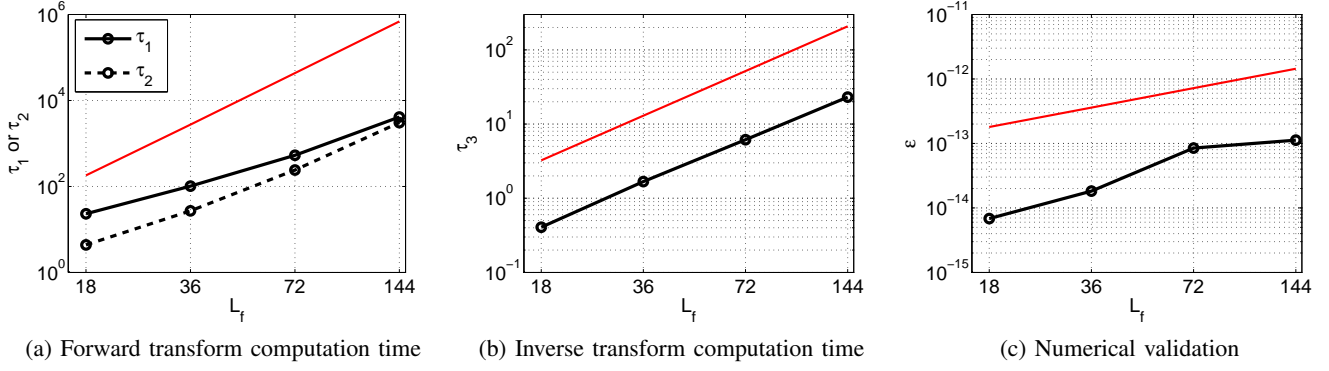


Fig. 6: Numerical validation and computation time of the proposed algorithms. (a) The computation time  $\tau_1$  (in seconds) is the time to compute all SLSHT distribution components of the test signal with band-limit  $L_f$  and is plotted for test signals of different band-limits. The computation time  $\tau_2$  denotes the time to compute the spherical harmonic transform of the modulated signal. Both  $\tau_1$  and  $\tau_2$  evolve as  $O(L_f^4)$  as shown by the solid red line. (b) The computation time  $\tau_3$  denotes the time to compute the inverse directional SLSHT, which scales as  $O(L_f^2)$  (for fix  $L_h$ ) as shown by the solid red line. (c) The maximum error  $\epsilon$  between the spherical harmonic coefficients of the test signal and those of the signal obtained via reconstruction from the SLSHT distribution components is plotted, which empirically appears to scale as  $O(L)$ , as shown by the solid red line.

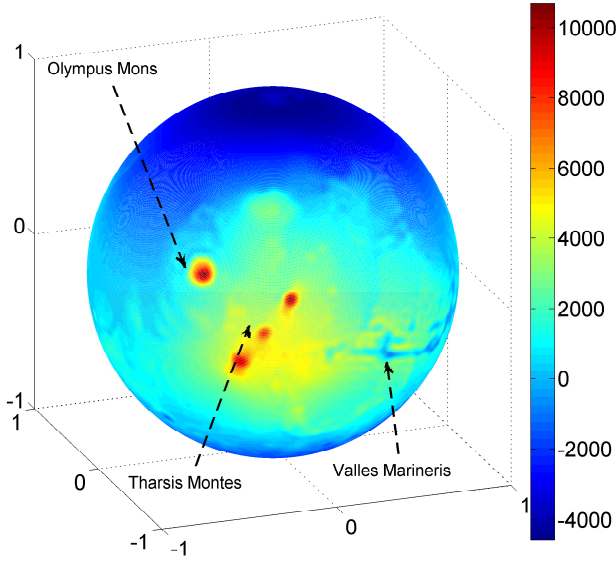


Fig. 7: Mars signal in the spatial domain. The grand canyon Valles Marineris and the mountainous regions of Tharsis Montes and Olympus Montes are indicated.

If we analyze the signal by employing the SLSHT using an azimuthally symmetric window function, the presence of localized contributions of higher degree spectral contents can be determined in the spatio-spectral domain [10], however the presence of directional features cannot be extracted. Here, we illustrate that the use

of the directional SLSHT enables the identification of directional features in the spatio-spectral domain, which is due to the consideration of an asymmetric window function for spatial localization.

We obtain the directional SLSHT distribution components  $g(\rho; \ell, m)$  of the Mars map  $f$  using the band-limited eigenfunction window  $h$  with  $L_h = 60$  and 90% concentration in the spatial domain in an ellipsoidal region  $\mathcal{R}_{(\pi/12, 7\pi/12)}$ . The SLSHT distribution components  $g(\rho; \ell, m)$  for order  $m = 15$  and degrees  $20 \leq \ell \leq 27$  and  $50 \leq \ell \leq 57$  are shown in Fig. 8 and Fig. 9 respectively, where the components in the panels are for Euler angle (a)  $\gamma = 0$  and (b)  $\gamma = 100\pi/201 = 1.5630 \approx \pi/2$ . Since the ellipsoidal region is oriented along the  $x$ -axis, the window with orientation  $\gamma = 0$  provides localization along colatitude and the window with orientation  $\gamma \approx \pi/2$  provides localization along longitude. It is evident that using orientation of the window  $\gamma \approx \pi/2$  probes the information about the grand canyon (directional feature) along longitude in the spatio-spectral domain. The localized contribution of higher degree spherical harmonics towards the mountainous region can also be observed in Fig. 8 for degree  $20 \leq \ell \leq 27$  and both  $\gamma = 0$  and  $\gamma = \pi/2$ . However, there is not significant contribution of spherical harmonics of degree  $50 \leq \ell \leq 57$  towards mountainous region as indicated in Fig. 9a where  $\gamma = 0$ , but the localization of the directional features along the orientation  $\gamma \approx \pi/2$  are revealed in the spatio-spectral domain as shown in Fig. 9b. Due to the ability of the

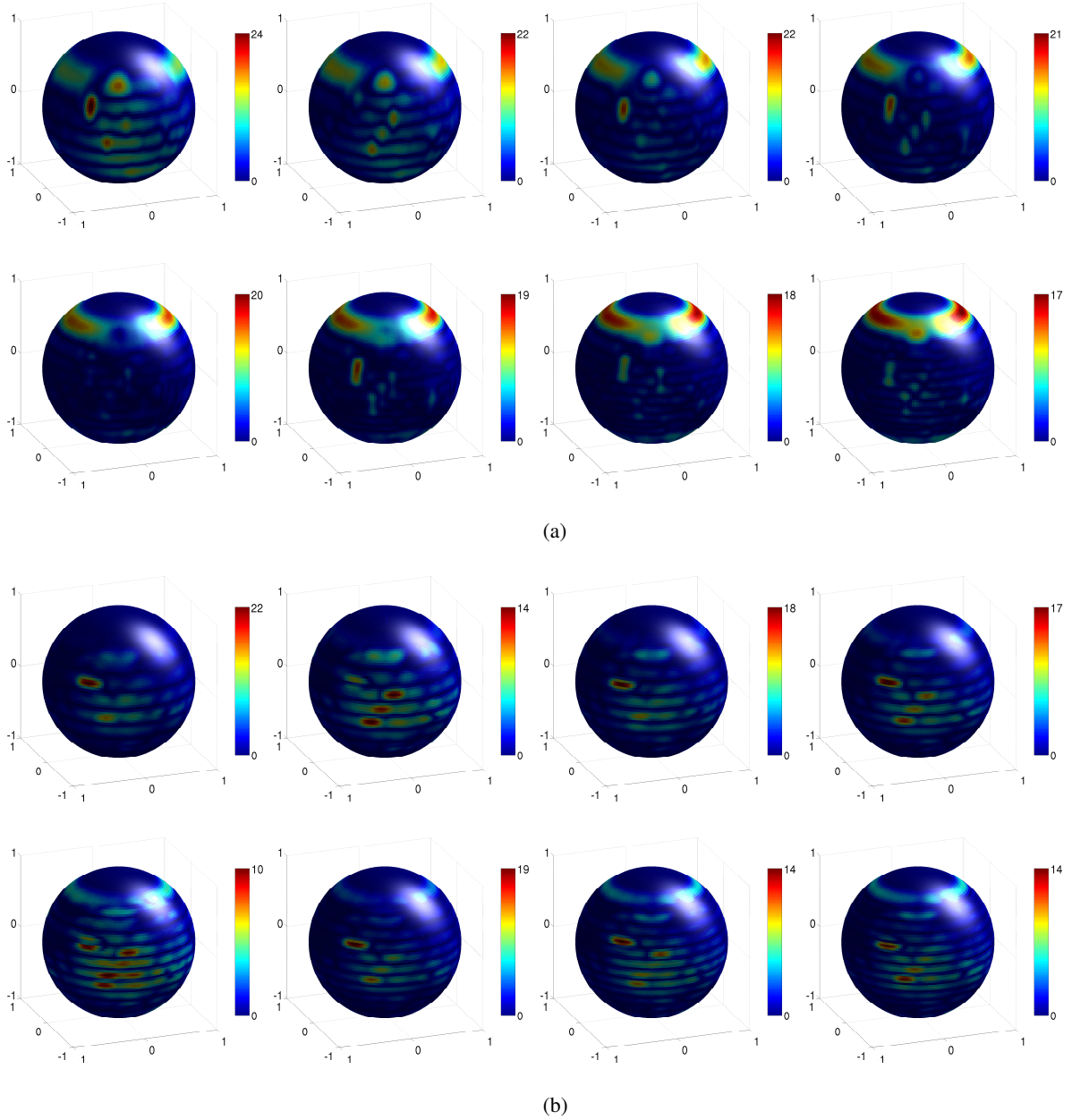


Fig. 8: Magnitude of the components of the directional SLSHT distribution of the Mars signal obtained using the eigenfunction window concentrated in an ellipsoidal region of focus  $\theta_c = \pi/12$  and major axis  $a = 7\pi/12$ . For fixed orientation  $\gamma$ , the distribution components  $g(\rho; \ell, m)$  are mapped on the sphere using  $\rho = (\phi, \theta, \gamma)$  for order  $m = 15$  and degree  $20 \leq \ell \leq 27$ . The components are shown for orientation (a)  $\gamma = 0$  and (b)  $\gamma \approx \pi/2$  of the window function around the  $z$ -axis. Top left:  $g(\rho; 20, 15)$ , top right:  $g(\rho; 23, 15)$ .

directional SLSHT to reveal the localized contribution of spectral contents and the directional or oriented features in the spatio-spectral domain, it can be useful in many applications where the signal on the sphere is localized in position and orientation.

## VII. CONCLUSIONS

We have presented the directional SLSHT to project a signal on the sphere onto its joint spatio-spectral domain as a directional SLSHT distribution. In spirit, the directional SLSHT is composed of SO(3) spatial localization

followed by the spherical harmonic transform. Here, we have proposed the use of an azimuthally asymmetric window function to obtain spatial localization, which enables the transform to resolve directional features in the spatio-spectral domain. We have also presented an inversion relation to synthesize the original signal from its directional SLSHT distribution. Since datasets on the sphere are of considerable size, we have developed a fast algorithm for the efficient computation of the directional SLSHT distribution of a signal. The computational complexity of computing the directional

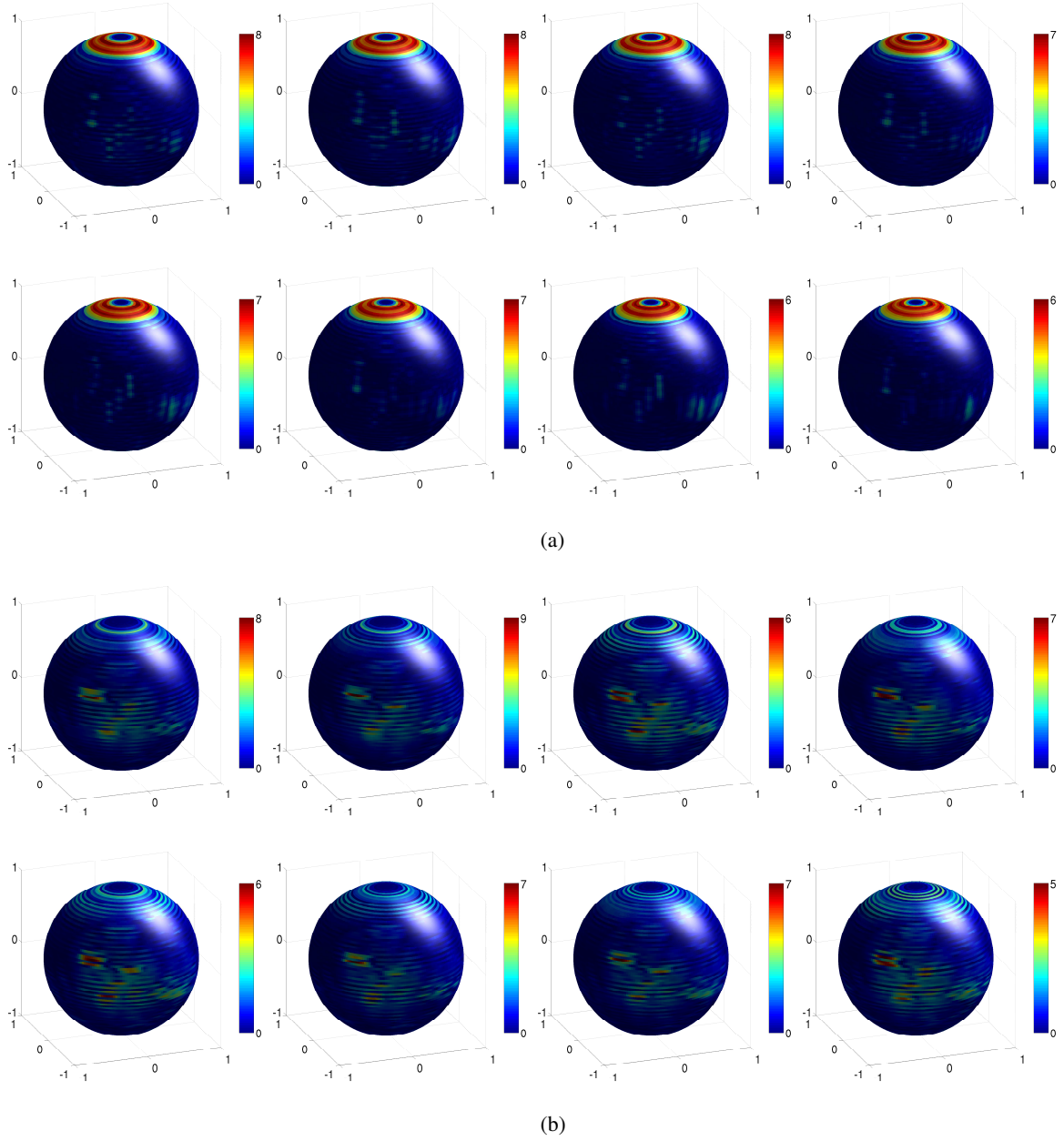


Fig. 9: Magnitude of the components of the directional SLSHT distribution of the Mars signal obtained using the eigenfunction window concentrated in an ellipsoidal region of focus  $\theta_c = \pi/12$  and major axis  $a = 7\pi/12$ . For fixed orientation  $\gamma$ , the distribution components  $g(\rho; \ell, m)$  are mapped on the sphere using  $\rho = (\phi, \theta, \gamma)$  for order  $m = 15$  and degree  $50 \leq \ell \leq 57$ . The components are shown for orientation (a)  $\gamma = 0$  and (b)  $\gamma \approx \pi/2$  of the window function around  $z$ -axis. Top left:  $g(\rho; 50, 15)$ , top right:  $g(\rho; 53, 15)$ .

SLSHT is reduced by providing an alternative harmonic formulation of the transform and then exploiting the factoring of rotation approach [41] and the fast Fourier transform. The computational complexity of the proposed fast algorithm to evaluate SLSHT distribution of a signal with band-limit  $L_f$  using window function with band-limit  $L_h$  is  $O(L_f^4 \min(\log_2 L_f, L_h) + L_f^2 L_h^4)$  as compared to the complexity of direct evaluation, which is  $O(L_f^4 L_h^3)$ . The numerical accuracy and the speed of our fast algorithm has also been studied. The directional SLSHT distribution relies on a window function for spa-

tial localization; we have analyzed the band-limited window function obtained from the Slepian concentration problem on the sphere, with nominal concentration in an ellipsoidal region around the north pole. We provided an illustration which highlighted the capability of the directional SLSHT to reveal directional features in the spatio-spectral domain.

There are natural extensions and applications of the work presented. Our directional SLSHT distribution can be used in many applications to resolve localized directional contents in a signal. Furthermore, the use of



the directional SLSHT transform to perform spatially-varying filtering of the directional features of a signal in the spatio-spectral domain needs to be studied [12]. Since the SLSHT is analogous in nature to the short-time Fourier transform (STFT) in time-frequency analysis [48], following the extension of the STFT presented in [49], [50], the use of different window functions for obtaining localization at different spatial positions presents an open problem for future work.

## APPENDIX A SPHERICAL HARMONIC TRANSFORM OF MODULATED SIGNAL

Our objective is to compute the spherical harmonic transform of the modulated signal  $\bar{f}Y_\ell^m$ , for given  $\ell$  and  $m$ , up to degree  $L_h$ , which can be performed in two ways. Firstly, we could use a simple separation variable technique given by

$$(\bar{f}Y_\ell^m)_p^q = N_\ell^m N_p^q \int_0^\pi P_\ell^m(\cos\theta) P_p^q(\cos\theta) \times \left( \int_0^{2\pi} \overline{f(\theta, \phi)} e^{m\phi - q\phi} d\phi \right) \sin\theta d\theta. \quad (39)$$

Since  $0 \leq \ell \leq L_f + L_h$ , we need to consider the modulated signal  $\bar{f}Y_\ell^m$  sampled on the grid  $\mathfrak{S}_{2L_f+2L_h}$  for the explicit evaluation of exact quadrature [35]. Using (39), the integral over  $\phi$  can be computed first in  $O(L_f^2)$  for each  $q$  and in  $O(L_f^2 L_h)$  for all  $|q| \leq L_h$ . We can also employ an FFT to evaluate the integral over  $\phi$  in  $O(L_f^2 \log_2 L_f)$  time. Then, using the exact quadrature weights derived in [35], the integral over  $\theta$  can be computed in  $O(L_f)$  for each  $p, q$  and for in  $O(L_f L_h^2)$  for all  $p, q$ . Thus the overall complexity using this approach is  $O(\max(\min(L_f^2 \log_2 L_f, L_f^2 L_h), L_f L_h^2)) \sim O(L_f^2 \min(\log_2 L_f, L_h))$ , since throughout we assume  $L_h \leq L_f$ . Alternatively, we can employ a factoring of rotation approach to compute the spherical harmonic transform according to the method given in [35], which has the complexity  $O(\max(L_f^2 \log_2 L_f, L_h^3)) \sim O(L_f^2 \log_2 L_f)$  but supports a sampling of the modulated signal on the lower resolution grid  $\mathfrak{S}_{2L_f+L_h}$ . Therefore, the spherical harmonic transform of the modulated signal  $\bar{f}Y_\ell^m$  up to degree  $L_h$  can be computed with asymptotic complexity  $O(L_f^2 \min(\log_2 L_f, L_h))$ .

## REFERENCES

- [1] M. K. Chung, K. J. Worsley, B. M. Nacewicz, K. M. Dalton, and R. J. Davidson, "General multivariate linear modeling of surface shapes using surfstat," *NeuroImage*, vol. 53, no. 2, pp. 491–505, 2010.
- [2] F. J. Simons, F. A. Dahlen, and M. A. Wieczorek, "Spatiospectral concentration on a sphere," *SIAM Rev.*, vol. 48, no. 3, pp. 504–536, 2006.
- [3] C. Han, B. Sun, R. Ramamoorthi, and E. Grinspun, "Frequency domain normal map filtering," *ACM Trans. on Graphics*, vol. 26, no. 3, pp. 28:1–28:12, Jul. 2007.
- [4] P. Audet, "Directional wavelet analysis on the sphere: Application to gravity and topography of the terrestrial planets," *J. Geophys. Res.*, vol. 116, Feb. 2011.
- [5] D. Colton and R. Kress, *Inverse Acoustic and Electromagnetic Scattering Theory*, 2nd ed. Berlin: Springer-Verlag, 1998.
- [6] D. N. Spergel, R. Bean, O. Doré, M. R. Nolta, C. L. Bennett, J. Dunkley, G. Hinshaw, N. Jarosik, E. Komatsu, L. Page, H. V. Peiris, L. Verde, M. Halpern, R. S. Hill, A. Kogut, M. Limon, S. S. Meyer, N. Odegard, G. S. Tucker, J. L. Weiland, E. Wollack, and E. L. Wright, "Three-year Wilkinson Microwave Anisotropy Probe (WMAP) observations: Implications for cosmology," *The Astrophysical Journal Supplement Series*, vol. 170, no. 2, pp. 377–408, 2007.
- [7] D. B. Ward, R. A. Kennedy, and R. C. Williamson, "Theory and design of broadband sensor arrays with frequency invariant far-field beam patterns," *J. Acoust. Soc. Am.*, vol. 97, no. 2, pp. 1023–1034, Feb. 1995.
- [8] T. S. Pollock, T. D. Abhayapala, and R. A. Kennedy, "Introducing space into MIMO capacity calculations," *J. Telecommun. Syst.*, vol. 24, no. 2, pp. 415–436, Oct. 2003.
- [9] J.-P. Antoine and P. Vandergheynst, "Wavelets on the 2-sphere: A group-theoretical approach," *Appl. Comput. Harmon. Anal.*, vol. 7, no. 3, pp. 262–291, 1999.
- [10] Z. Khalid, S. Durrani, P. Sadeghi, and R. A. Kennedy, "Spatio-spectral analysis on the sphere using spatially localized spherical harmonics transform," *IEEE Trans. Signal Process.*, vol. 60, no. 3, pp. 1487–1492, Mar. 2012.
- [11] Z. Khalid, S. Durrani, R. A. Kennedy, and P. Sadeghi, "Conjugate gradient algorithm for extrapolation of sampled bandlimited signals on the 2-sphere," in *Proc. IEEE Int. Conf. Acoust., Speech, Signal Process., ICASSP'2012*, Kyoto, Japan, Mar. 2011.
- [12] Z. Khalid, P. Sadeghi, R. A. Kennedy, and S. Durrani, "Spatially varying spectral filtering of signals on the unit sphere," *IEEE Trans. Signal Process.*, 2012, (under second round of review).
- [13] D. Marinucci, D. Pietrobon, A. Balbi, P. Baldi, P. Cabella, G. Kerkycharian, P. Natoli, D. Picard, and N. Vittorio, "Spherical needlets for cosmic microwave background data analysis," *Mon. Not. R. Astron. Soc.*, vol. 383, no. 2, pp. 539–545, 2008.
- [14] J. D. McEwen, M. P. Hobson, and A. N. Lasenby, "A directional continuous wavelet transform on the sphere," *Arxiv preprint astro-ph/0609159*, 2006.
- [15] J. D. McEwen, M. P. Hobson, D. J. Mortlock, and A. N. Lasenby, "Fast directional continuous spherical wavelet transform algorithms," *IEEE Trans. Signal Process.*, vol. 55, no. 2, pp. 520–529, Feb. 2007.
- [16] J. McEwen, M. Hobson, and A. Lasenby, "Optimal filters on the sphere," *IEEE Trans. Signal Process.*, vol. 56, no. 8, pp. 3813–3823, Aug. 2008.
- [17] P. Sadeghi, R. A. Kennedy, and Z. Khalid, "Commutative anisotropic convolution on the 2-sphere," *IEEE Trans. Signal Process.*, 2012, (under second round of review).
- [18] M. Simons, S. C. Solomon, and B. H. Hager, "Localization of gravity and topography: constraints on the tectonics and mantle dynamics of venus," *Geophys. J. Int.*, vol. 131, no. 1, pp. 24–44, Oct. 1997.
- [19] J.-L. Starck, Y. Moudden, P. Abrial, and M. Nguyen, "Wavelets, ridgelets and curvelets on the sphere," *Astron. & Astrophys.*, vol. 446, no. 3, pp. 1191–1204, Feb. 2006.
- [20] Y. Wiaux, L. Jacques, and P. Vandergheynst, "Correspondence principle between spherical and Euclidean wavelets," *Astrophys. J.*, vol. 632, no. 1, pp. 15–28, Oct. 2005.

- [21] Y. Wiaux, L. Jacques, P. Vielva, and P. Vanderghelynst, "Fast directional correlation on the sphere with steerable filters," *Astrophys. J.*, vol. 652, no. 1, pp. 820–832, Nov. 2006.
- [22] Y. Wiaux, J. D. McEwen, P. Vanderghelynst, and O. Blanc, "Exact reconstruction with directional wavelets on the sphere," *Mon. Not. R. Astron. Soc.*, vol. 388, no. 2, pp. 770–788, 2008.
- [23] B. T. T. Yeo, W. Ou, and P. Golland, "On the construction of invertible filter banks on the 2-sphere," *IEEE Trans. Image Process.*, vol. 17, no. 3, pp. 283–300, Mar. 2008.
- [24] R. B. Barreiro, M. P. Hobson, A. N. Lasenby, A. J. Banday, K. M. Górski, and G. Hinshaw, "Testing the Gaussianity of the COBE DMR data with spherical wavelets," *Mon. Not. R. Astron. Soc.*, vol. 318, pp. 475–481, Oct. 2000.
- [25] J. D. McEwen, M. P. Hobson, A. N. Lasenby, and D. J. Mortlock, "A high-significance detection of non-Gaussianity in the Wilkinson Microwave Anisotropy Probe 1-yr data using directional spherical wavelets," *Mon. Not. R. Astron. Soc.*, vol. 359, no. 4, pp. 1583–1596, 2005.
- [26] J. D. McEwen, P. Vielva, Y. Wiaux, R. B. Barreiro, L. Cayón, M. P. Hobson, A. N. Lasenby, E. Martínez-González, and J. L. Sanz, "Cosmological applications of a wavelet analysis on the sphere," *J. Fourier Anal. and Appl.*, vol. 13, no. 4, pp. 495–510, Aug. 2007.
- [27] D. Pietrobon, A. Amblard, A. Balbi, P. Cabella, A. Cooray, and D. Marinucci, "Needlet detection of features in the WMAP CMB sky and the impact on anisotropies and hemispherical asymmetries," *Phys. Rev. D*, vol. 78, no. 10, p. 103504, Nov. 2008.
- [28] J. Schmitt, J. L. Starck, J. M. Casandjian, J. Fadili, and I. Grenier, "Poisson denoising on the sphere: application to the Fermi gamma ray space telescope," *Astron. & Astrophys.*, vol. 517, p. A26, Jul. 2010.
- [29] P. Vielva, E. Martínez-González, R. B. Barreiro, J. L. Sanz, and L. Cayón, "Detection of non-Gaussianity in the WMAP 1-year data using spherical wavelets," *Astrophys. J.*, vol. 609, pp. 22–34, 2004.
- [30] F. J. Simons, I. Loris, G. Nolet, I. C. Daubechies, S. Voronin, P. A. Vetter, J. Charly, and C. Vonesch, "Solving or resolving global tomographic models with spherical wavelets, and the scale and sparsity of seismic heterogeneity," *Geophys. J. Int.*, vol. 187, pp. 969–988, 2011.
- [31] F. J. Simons, I. Loris, E. Brevdo, and I. C. Daubechies, "Wavelets and wavelet-like transforms on the sphere and their application to geophysical data inversion," in *Wavelets and Sparsity XIV*, vol. 81380. SPIE, 2011, p. 81380X.
- [32] M. A. Wiczorek and F. J. Simons, "Localized spectral analysis on the sphere," *Geophys. J. Int.*, vol. 162, no. 3, pp. 655–675, May 2005.
- [33] —, "Minimum variance multitaper spectral estimation on the sphere," *J. Fourier Anal. Appl.*, vol. 13, no. 6, pp. 665–692, 2007.
- [34] J. R. Driscoll and D. M. Healy, Jr., "Computing Fourier transforms and convolutions on the 2-sphere," *Adv. Appl. Math.*, vol. 15, no. 2, pp. 202–250, Jun. 1994.
- [35] J. McEwen and Y. Wiaux, "A novel sampling theorem on the sphere," *IEEE Trans. Signal Process.*, vol. 59, no. 12, pp. 5876–5887, Dec. 2011.
- [36] J. J. Sakurai, *Modern Quantum Mechanics*, 2nd ed. Reading, MA: Addison Wesley Publishing Company, Inc., 1994.
- [37] N. Jarosik, C. L. Bennett, J. Dunkley, B. Gold, M. R. Greason, M. Halpern, R. S. Hill, G. Hinshaw, A. Kogut, E. Komatsu, D. Larson, M. Limon, S. S. Meyer, M. R. Nolte, N. Odegard, L. Page, K. M. Smith, D. Spergel, G. S. Tucker, J. L. Weiland, E. Wollack, and E. L. Wright, "Seven-year Wilkinson Microwave Anisotropy Probe (WMAP) observations: Sky maps, systematic errors, and basic results," *Astrophys. J.*, vol. 192, no. 2, pp. 1–14, 2011.
- [38] Planck collaboration, "ESA Planck blue book," ESA, Tech. Rep. ESA-SCI(2005)1, 2005.
- [39] R. A. Kennedy, T. A. Lamahewa, and L. Wei, "On azimuthally symmetric 2-sphere convolution," *Digital Signal Processing*, vol. 5, no. 11, pp. 660–666, Sep. 2011.
- [40] D. A. Varshalovich, A. N. Moskalev, and V. K. Khersonskii, *Quantum Theory of Angular Momentum*. World Scientific, 1988.
- [41] T. Risbo, "Fourier transform summation of Legendre series and D-functions," *J. Geodesy*, vol. 70, pp. 383–396, 1996.
- [42] B. D. Wandelt and K. M. Górski, "Fast convolution on the sphere," *Phys. Rev. D*, vol. 63, no. 12, p. 123002, May 2001.
- [43] S. Trapani and J. Navaza, "Calculation of spherical harmonics and wigner  $d$  functions by fft. applications to fast rotational matching in molecular replacement and implementation into *amore*," *Acta Crystallogr. Sect. A*, vol. 62, no. 4, pp. 262–269, Jul. 2006.
- [44] W. Freedman and V. Michel, "Constructive approximation and numerical methods in geodetic research today – an attempt at a categorization based on an uncertainty principle," *J. Geodesy*, vol. 73, no. 9, pp. 452–465, 1999.
- [45] L. Cohen, "Time-frequency distributions-a review," *Proc. IEEE*, vol. 77, no. 7, pp. 941–981, Jul. 1989.
- [46] Z. Khalid, S. Durrani, R. Kennedy, and P. Sadeghi, "Revisiting slepian concentration problem on the sphere for azimuthally non-symmetric regions," in *5th International Conference on Signal Processing and Communication Systems, ICSPCS'2011*, Honolulu, HI, Dec. 2011.
- [47] F. J. Narcowich and J. D. Ward, "Nonstationary wavelets on the  $m$ -sphere for scattered data," *Appl. Comput. Harmon. Anal.*, vol. 3, no. 4, pp. 324–336, Oct. 1996.
- [48] L. Cohen, *Time-frequency analysis: Theory and applications*. Prentice-Hall, Inc., 1995.
- [49] R. Czerwinski and D. Jones, "Adaptive short-time fourier analysis," *IEEE Signal Process. Lett.*, vol. 4, no. 2, pp. 42–45, Feb. 1997.
- [50] J. Zhong and Y. Huang, "Time-frequency representation based on an adaptive short-time Fourier transform," *IEEE Trans. Signal Process.*, vol. 58, no. 10, pp. 5118–5128, Oct. 2010.



**Zubair Khalid** (S'10) received his B.Sc. (first-class hon.) degree in Electrical Engineering from the University of Engineering & Technology (UET), Lahore, Pakistan in 2008. He is currently pursuing his PhD degree from the Research School of Engineering, the Australian National University, Canberra, Australia. Zubair was awarded University Gold Medal and Industry Gold Medals from Siemens and Nespak for his overall outstanding performance in Electrical Engineering during the his undergraduate studies. He is a recipient of an Endeavour International Postgraduate Award for the duration of his Ph.D. He was also awarded an ANU Vice Chancellors Higher Degree Research (HDR) travel grant in 2011. His research interests are in the area of development of novel signal processing techniques for signals on the sphere.





**Rodney A. Kennedy** (S'86-M'88-SM'01-F'05) received the B.E. degree from the University of New South Wales, Sydney, Australia, the M.E. degree from the University of Newcastle, and the Ph.D. degree from the Australian National University, Canberra.

He is currently a Professor in the Research School of Engineering, Australian National University. He is a Fellow of the IEEE. His research interests include digital signal processing, digital and wireless communications, and acoustical signal processing.



**Salman Durrani** (S'00-M'05-SM'10) received the B.Sc. (1st class honours) degree in Electrical Engineering from the University of Engineering & Technology, Lahore, Pakistan in 2000. He received the PhD degree in Electrical Engineering from the University of Queensland, Brisbane, Australia in Dec. 2004. He has been with the Australian National University, Canberra, Australia, since 2005,

where he is currently a Senior Lecturer in the Research School of Engineering, College of Engineering & Computer Science.

His current research interests are in wireless communications and signal processing, including synchronization in cooperative communication systems, connectivity of ad-hoc networks and vehicular networks and signal processing on the unit sphere. He serves as a Technical Program Committee Member for international conferences such as ICC '13, PIMRC '12 and AusCTW '12. He was awarded an ANU Vice-Chancellor's Award for Teaching Excellence in 2012. He was a recipient of an International Postgraduate Research Scholarship from the Australian Commonwealth during 2001-2004. He was awarded a University Gold Medal during his undergraduate studies. He has 55 publications to date in refereed international journals and conferences. He is a Member of Institution of Engineers, Australia and a Senior Member of IEEE.



**Parastoo Sadeghi** (S'02-M'06-SM'07) received the B.E. and M.E. degrees in electrical engineering from Sharif University of Technology, Tehran, Iran, in 1995 and 1997, respectively, and the Ph.D. degree in electrical engineering from The University of New South Wales, Sydney, Australia, in 2006. From 1997 to 2002, she worked as a Research Engineer and then as a Senior Research Engineer at

Iran Communication Industries (ICI) in Tehran, Iran and at Deqx (formerly known as Clarity Eq) in Sydney, Australia. She is currently a Fellow at the Research School of Engineering, The Australian National University, Canberra, Australia. She has visited various research institutes, including the Institute for Communications Engineering, Technical University of Munich, from April to June 2008 and MIT from February to May 2009.

Dr. Sadeghi has co-authored more than 80 refereed journal or conference papers and is a Chief Investigator in a number of Australian Research Council Discovery and Linkage Projects. In 2003 and 2005, she received two IEEE Region 10 student paper awards for her research in the information theory of time-varying fading channels. Her research interests are mainly in the area of wireless communications systems and signal processing.



**Jason McEwen** received a B.E. (Hons) degree in Electrical and Computer Engineering from the University of Canterbury, New Zealand, in 2002 and a Ph.D. degree in Astrophysics from the University of Cambridge in 2007.

He held a Research Fellowship at Clare College, Cambridge, from 2007 to 2008, worked as a Quantitative Analyst from 2008 to 2010, and held a position as a Postdoctoral Researcher at Ecole Polytechnique Fédérale de Lausanne (EPFL), Switzerland, from 2010 to 2011. From 2011 to 2012 he held a Leverhulme Trust Early Career Fellowship at University College London (UCL), where he remains as a Newton International Fellow, supported by the Royal Society and the British Academy. His research interests are focused on spherical signal processing, including sampling theorems and wavelets on the sphere, compressed sensing and Bayesian statistics, and applications of these techniques to cosmology and radio interferometry.